HHS Public Access

Author manuscript

Magn Reson Med. Author manuscript; available in PMC 2016 February 07.

Published in final edited form as:

Magn Reson Med. 2015 July ; 74(1): 93–105. doi:10.1002/mrm.25377.

Improved Quantitative Myocardial T_2 Mapping

Mehmet Akçakaya[1], **Tamer A. Basha**[1], **Sebastian Weingärtner**[1,2], **Sébastien Roujol**[1], **Sophie Berg**[1], and **Reza Nezafat**[1]

[1]Department of Medicine (Cardiovascular Division), Beth Israel Deaconess Medical Center and Harvard Medical School, Boston, MA

[2]Computer Assisted Clinical Medicine, University Medical Center Mannheim, Heidelberg University, Mannheim, Germany

Abstract

Purpose—To develop an improved T_2 prepared (T_2prep) balanced steady-state free-precession (bSSFP) sequence and signal relaxation curve fitting method for myocardial T_2 mapping.

Methods—Myocardial T_2 mapping is commonly performed by acquisition of multiple T_2prep bSSFP images and estimating the voxel-wise T_2 values using a 2-parameter fit for relaxation. However, a 2-parameter fit model does not take into account the effect of imaging pulses in a bSSFP sequence or other imperfections in T_2prep RF pulses, which may decrease the robustness of T_2 mapping. Therefore, we propose a novel T_2 mapping sequence that incorporates an additional image acquired with saturation preparation, simulating a very long T_2prep echo time. This enables the robust estimation of T_2 maps using a 3-parameter fit model, which captures the effect of imaging pulses and other imperfections. Phantom imaging is performed to compare the T_2 maps generated using the proposed 3-parameter model to the conventional 2-parameter model, as well as a spin echo reference. In-vivo imaging is performed on eight healthy subjects to compare the different fitting models.

Results—Phantom and in-vivo data show that the T_2 values generated by the proposed 3-parameter model fitting do not change with different choices of the T_2prep echo times, and are not statistically different than the reference values for the phantom ($P = 0.10$ with three T_2prep echoes). The 2-parameter model exhibits dependence on the choice of T_2prep echo times and are significantly different than the reference values ($P = 0.01$ with three T_2prep echoes).

Conclusion—The proposed imaging sequence in combination with a 3-parameter model allows accurate measurement of myocardial T_2 values, which is independent of number and duration of T_2prep echo times.

Keywords

Quantitative myocardial tissue characterization; myocardial T_2 mapping; 3-parameter fit; myocardial inflammation

Correspondence to: Reza Nezafat, Ph. D., Beth Israel Deaconess Medical Center, 330 Brookline Ave, Boston, MA, 02215, Phone: 617-667-1747; Fax: 617-975-5480, rnezafat@bidmc.harvard.edu.

The first two authors contributed equally to this work.

Introduction

T_2-weighted images are commonly used in cardiac MR (CMR) to assess myocardial inflammation and edema in various cardiomyopathies. They have been shown to distinguish acute and chronic myocardial infarction (1), to identify severe transient myocardial ischemia (2), and to predict revascularization needs (3). T_2-weighted imaging has also been used in patients with myocarditis (4,5), allograft rejection (6) and Takotsubo cardiomyopathy (7), where T_2 values are elevated. The T_2-weighted imaging sequences used in these studies rely on turbo spin echo readouts with black-blood preparation (8). However, the T_2-weighted imaging sequences suffer from certain limitations (9-11), including qualitative interpretation that is affected by regional differences; myocardial signal variation due to phased-array coil arrays; and difficulty differentiating edema from stagnant sub-endocardial blood.

Quantification of myocardial T_2 values (12,13) has been proposed as an alternative to T_2-weighted imaging to reduce the variation in assessment. The earlier T_2 quantification sequences were based on spin echo/fast spin echo acquisitions (12-15). More recently, T_2 mapping techniques (11,16-20) have been proposed, where a number of images are acquired with different T_2-weightings, and used to generate a quantitative pixel-wise T_2 map based on a spin-spin relaxation model compatible with the acquisition. T_2-prepared (21) balanced steady-state free precession (bSSFP) techniques have been utilized for efficient T_2 mapping (22). In these techniques, a number of different T_2 preparation (T_2prep) echo times are used to generate the multiple T_2-weighted images (11,16-20). In one such approach, three electrocardiogram (ECG)-triggered single-shot bSSFP images are acquired with three different T_2prep times (0 ms, 24 ms, 55 ms) with 2 heart-beat rest periods for signal recovery between each image, using a breath-hold acquisition (11,18). These images are subsequently registered and then fit to a 2-parameter fit model (consisting of the longitudinal magnetization without T_2prep and the T_2 time) to generate the myocardial T_2 maps.

Despite the potential of myocardial T_2 mapping for quantitative assessment of myocardial inflammation and edema (18,19,23-26), it has still not replaced T_2-weighted techniques in clinical CMR protocols. In terms of the sequence, single-shot bSSFP acquisitions following different T_2prep echo times have replaced the spin echo approach. However, there is a lack of data about the robustness of T_2 estimation with respect to the choice and number of T_2prep echo times when using the conventional sequences and the curve fitting model.

In terms of the curve-fitting model, the 2-parameter fit has been used extensively in the literature, both with spin echo acquisitions (12,14,27) or bSSFP acquisitions with various profile ordering schemes (16,20,22). However, the 2-parameter model ignores the changes in the T_1/T_2 contrast due to the imaging pulses until the acquisition of the center of k-space when using a bSSFP sequence, with a number of start-up pulses and especially with linear profile ordering. The shortcomings of the 2-parameter model have been noted previously (17,28). In (17), an empirical offset parameter was included to account for the T_1 relaxation during the gradient echo sequence. This value was chosen based on Bloch simulations and was fixed for a given set of sequence parameters and physiology characteristics. In (28), a third parameter was empirically included to characterize the deviations from the 2-parameter

model in numerical simulations and phantom experiments, although no analytical insight was given regarding the necessity of such a term.

In this work, we propose a sequence and a signal recovery curve fitting model for improved myocardial T_2 mapping. We propose a 3-parameter curve fitting model, where the third parameter captures the perturbations in the magnetization curve due to the imaging pulses played between the T_2prep and the acquisition of the central k-space line. Our proposed sequence acquires multiple single-shot images with different T_2prep echo times, followed by rest periods for magnetization recovery, as well as one saturation-prepared image. The latter captures the effect of imaging pulses on the magnetization curve, and thus improves the estimation of the third parameter. Additionally, to enable efficient free-breathing acquisitions in-vivo, we propose a new NAV-gating scheme that applies T_2prep conditionally based on the position of the NAV signal. This eliminates the necessity for rest periods if the NAV signal is outside of the gating window. Phantom experiments and in vivo imaging are performed to evaluate the proposed sequence and the recovery curve fitting model.

Methods

The 2-parameter curve fitting model typically used in myocardial T_2 mapping is given by

$$M_{2\text{-parameter}}(t) = Ae^{-t/T_2}, \quad [1]$$

where t is the T_2prep echo time. In this work, we propose to use a 3-parameter model to capture the effect of imaging pulses on the magnetization

$$M_{3\text{-parameter}}(t) = Ae^{-t/T_2} + B. \quad [2]$$

The proposed sequence aims to improve the efficiency and accuracy of T_2 mapping, while addressing several aspects of this estimation procedure.

Proposed Sequence

Figure 1(a) shows the schematic of the proposed sequence. Multiple single-shot images of the heart are acquired using ECG-triggering, following T_2prep (21) of different echo lengths, TE_{T2P}. Between each image, a 6 second rest period (with no RF pulses) is applied to allow for full re-growth of the myocardial signal. To improve the estimation of the third parameter (B), the sequence additionally acquires an image, I_{SAT}, directly after a saturation pulse to simulate the effect of a very long T_2prep echo time (i.e. T_2prep = ∞).

The T_2prep itself consists of 90° tip-down pulse, followed by four 180° pulses and ends with 90° tip-up pulse. Both the opening and closing 90° pulses are non-selective hard pulses with a bandwidth of 2.3 kHz, and duration of 0.44 ms. These non-composite short pulses were chosen to minimize any T_2* effect that might occur during the pulse. The refocus pulses are

weighted in a MLEV opposing phase pairs scheme to compensate for RF pulse shape imperfection (29) and composite refocusing pulses ($90°_x$, $180°_y$, $90°_x$) are used to provide second order corrections to variations in B_1. The duration of each refocus pulse is 1.75 ms. For I_{SAT}, a composite saturation pulse of bandwidth = 1 kHz, and a total duration of 10 ms is used.

A common issue with T_2prep sequences is the effect of B_0 and B_1 variations of the excitation and refocusing pulses of the T_2prep sequence. In the proposed method, this will change the A parameter in Equation [2] for all the images acquired with a non-zero TE_{T2P}. However, if $TE_{T2P} = 0$ is acquired with no contrast preparation as in (11), the A parameter for this term will not be affected by these in homogeneity effects, leading to an inconsistency with the other TE_{T2P} values. To compensate for this effect, we add a 90°, followed immediately by a -90°, followed by a crusher gradient, for the acquisition of a $TE_{T2P} = 0$, similar to the one proposed in (22). We hypothesize that this compensates for B_0 and B_1 variations, and removes the bias from the estimation of the T_2 parameter that would have been caused by RF flip angle imperfections.

The flowchart for the proposed navigator-gated acquisition scheme is depicted in Figure 1(b). The NAV is placed immediately prior to the T_2prep. For the acquisition of the k^{th} image, I_k, if the NAV signal is outside the gating window, no T_2prep or imaging pulses are applied, leaving the magnetization undisturbed, and the acquisition of I_k is repeated in the next R-R interval. If the NAV signal is within the gating window, the image with the desired T_2prep time is acquired, followed by a 6 second rest period for magnetization recovery. Figure 1(c) shows an example of the rejection-reacquisition scheme for a T_2-prepared image. Figure 1(d) also depicts the acquisition of a saturation-prepared (SAT) image, which immediately follows the T_2-prepared image without any rest periods, and where the NAV is placed prior to the saturation pulse.

3-parameter Model for T_2 Relaxation

We sought to characterize the effect of the bSSFP imaging pulses that are played until the acquisition of central k-space, on the magnetization measured after T_2 preparation. When a T_2prep scheme (21) with a T_2 echo time of TE_{T2P} is used, the longitudinal magnetization is given by:

$$M_{start} = M_0 e^{-TE_{T2P}/T_2}, \quad [3]$$

where M_0 is the signal at full-recovery. When using a bSSFP readout with n RF pulses, the signal is given by (30)

$$M(n) = [\sin(\alpha/2) M_{start} - M_{SS}]\lambda_1^n + M_{SS}, \quad [4]$$

where α is the flip angle, and where the steady state magnetization, M_{SS} is given by

$$M_{SS} = M_0 \frac{\sqrt{E_2}(1 - E_1) \sin(\alpha)}{1 - (E_1 - E_2)\cos(\alpha) - E_1 E_2}, \quad [5]$$

with $E_{1,2} = e^{-TR/T1,2}$ and $\lambda_1 = E_2 \sin^2(\alpha/2) + E_1 \cos^2(\alpha/2)$. This can be re-written as (31)

$$M(n) = \sin(\alpha/2)\lambda_1^n M_{start} + [1 - \lambda_1^n]M_{SS} = (M_0 \sin(\alpha/2)\lambda_1^n)e^{-TE_{T2P}/T_2} + [1 - \lambda_1^n]M_{SS}. \quad [6]$$

Thus, for T_2-prepared bSSFP acquisitions, in which several imaging pulses are used before the acquisition of the center of k-space, the T_2 relaxation between the different images can be characterized as:

$$M_{3\text{-parameter}}(TE_{T2P}) = Ae^{-TE_{T2P}/T_2} + B, \quad [7]$$

where the parameters, A and B do not depend on the T_2prep time, TE_{T2P}. However, they are functions of the sequence parameters (flip angle, number of pulses, repetition time, etc). Furthermore, based on Equation [6], we note that B captures the effect of the imaging pulses, when $M_{start} = 0$.

T_2 Map Reconstruction

T_2 maps are generated by voxel-wise least-squares curve-fitting to the magnitude signal intensity. Both the 2-parameter model in Equation [1] and the 3-parameter model in Equation [2] are utilized. The following curve-fitting methods are performed for the experiments:

1. The 2-parameter model with various T_2prep echo times. This method does not include the SAT image, since the 2-parameter signal model decays to 0 for large T_2prep echo times.
2. The 3-parameter model with various T_2prep echo times and with the saturation-prepared image. The SAT image is equivalently characterized as a long (~2000 ms) T_2prep echo time.
3. The 3-parameter model with various T_2prep echo times and without the SAT image.

Numerical Simulations: B_1 field inhomogeneity

Numerical simulations were conducted to study the effect of B_0 and B_1 variations on the estimated T_2 values, and to characterize the effect of using the proposed 90°, -90° and crusher gradient preparation during the acquisition of a $TE_{T2P} = 0$ on these T_2 estimations.

Bloch equation was simulated to consider the effect of spin rotation around B_{eff} instead of B_1 during the 90°, -90° and 180° pulses of the T_2prep, with

$$B_{eff} = B_1\hat{i} + \left(B_0 - \frac{\omega}{\gamma}\right)\hat{k}, \quad [8]$$

where B_0 is the strength of the magnetic field in the z-direction, γ is the gyromagnetic ratio, and B_1 and ω are the strength and frequency of the applied RF pulse respectively.

Nominal myocardium T_1 and T_2 values (i.e. 1200 ms and 50 ms respectively) were assumed for the simulations. The sequence was simulated to acquire T_2prep echo times of 0, 25 and 50 ms, as well as the saturation-prepared image. Then, both the 2-parameter and 3-parameter fits were used to estimate the T_2 values, and the absolute error from the true T_2 value was recorded for different variations of B_0 and B_1. The simulation was repeated with and without the proposed compensation for $TE_{T2P} = 0$.

Phantom Imaging

All imaging was performed on a 1.5T Philips Achieva (Philips Healthcare, Best, The Netherlands) system using a 32-channel cardiac coil array. Phantom imaging was performed using $NiCl_2$ doped agarose vials, whose T_2 and T_1 values spanned the ranges of values found in the blood and myocardium. A single-shot ECG-triggered bSSFP sequence with the following parameters was used for the proposed sequence: 2D single-slice, FOV = 240×240 mm^2, in-plane resolution = 2.5×2.5 mm^2, slice thickness = 8 mm, TR/TE = 2.7 ms/1.35 ms, flip angle = 85°, 10 linear ramp-up pulses, SENSE rate = 2, acquisition window = 138 ms, number of phase encoding lines = 51, linear k-space ordering. A total of 27 different T_2prep echo times were used, including $TE_{T2P} = 0$ and TE_{T2P} ranging from 25 ms to 150 ms in steps of 5 ms. Additionally one image was acquired after saturation preparation for the 3-parameter fit.

A Carr-Purcell-Meiboom-Gill (CPMG) spin-echo sequence with an echo train length of 32 with TE 10 ms was performed as reference. The scan parameters were: FOV = 240×240 mm^2, in-plane resolution = 1.25×1.25 mm^2, slice thickness = 4 mm, TR = 6000 ms, flip angle = 90°. Number of averages = 4, reference T_2 times were obtained from a 2-parameter model fit to the spin echo signal.

3-parameter vs. 2-parameter Fit: Effect of T_2prep Echo Times—We hypothesized that the estimated T_2 values would be independent of the T_2prep times used to sample the images if the true magnetization model and the curve-fitting model matched. On the other hand, the estimated T_2 values would change based on the T_2prep times sampled if there was mismatch between the true magnetization model and the curve-fitting model. To test this hypothesis, 2-parameter and 3-parameter models were used to generate T_2 maps based on different subsets of images corresponding to different T_2prep echo times. The following subsets were used:

a. TE_{T2P} = 0 and *n* TE_{T2P} values starting from 25ms in steps of 5 ms (*n* from 2 to 26).

b. TE_{T2P} = 0 and *n* TE_{T2P} values starting from 25 ms in steps of 10 ms (*n* from 2 to 13).

c. TE_{T2P} = 0 and *n* TE_{T2P} values starting from 25 ms in steps of 15 ms (*n* from 2 to 9).

d. TE_{T2P} = 0 and *n* TE_{T2P} values starting from 25 ms in steps of 20 ms (*n* from 2 to 7).

e. TE_{T2P} = 0 and *n* TE_{T2P} values starting from 25 ms in steps of 25 ms (*n* from 2 to 6).

As described previously, the additional SAT image is used with the 3-parameter model, and not used with the 2-parameter model. In order to quantify the effect of using the SAT image in the 3-parameter fit on accuracy and precision, these experiments were also repeated using the 3-parameter model but excluding the SAT image from the curve-fitting process.

Additionally, T_2 map estimation was performed using 3 T_2prep echoes (0, 25, 50 ms), similar to the ones used in the literature (11,17,18) using a 2-parameter fit. 3-parameter fit was performed using these 3 echoes and the proposed SAT image. 3-parameter fit was also performed using a 4^{th} echo at 90 ms instead of the SAT image. These acquisitions are referred to as the short acquisition with 2-parameter, 3-parameter fit with SAT, and 3-parameter without SAT, respectively.

Effect of the B_1 inhomogeneities—To quantify the effect of using the 90°, -90°& crusher gradient preparation during the acquisition of a TE_{T2P} = 0 to compensate for any RF pulse imperfection, imaging was performed with and without (i.e. no pulses applied) this correction. The 2-parameter and 3-parameter fits were performed for all echoes for both acquisitions. An additional SAT image was used for the 3-parameter fit as previously described.

Length of the Rest Cycles—Rest cycles are used after the acquisition of each single-shot image to allow for magnetization recovery. Imaging was performed to study the effect of the length of these rest cycles, using rest cycle lengths varying from 0 to 9 seconds in 1 second-steps. Imaging was performed using both 3 echoes (0, 25, 50 ms) and 27 echoes. An additional SAT image was acquired in all cases. The 3-parameter fit was utilized for T_2 map reconstruction.

T_2 Map Analysis—A region-of-interest (ROI) analysis was performed, where the mean value and standard deviation was recorded for each vial for each calculated T_2 map. Accuracy was assessed as the difference between the mean of the vial for the spin echo reference T_2 map and the mean of the vial for the given T_2 map. Precision was assessed as the standard deviation of the vial for the given T_2 map. The null hypotheses that there was no difference in the mean value for a vial in the spin echo reference and in a given T_2 map

was tested using a paired t-test across all vials. A *P* value of <0.05 was considered to be significant.

In Vivo Imaging

This portion of the study was approved by the institutional review board and written informed consent was acquired prior to each examination. In a prospective study, eight healthy adult subjects (30.3 ± 17.5 years, range: 22 - 73 years, 4 men) without contraindications to MRI were recruited. For each subject, localizer scouts were acquired to define the mid-ventricular short-axis slice. A two-dimensional spiral NAV echo was positioned on the right hemi-diaphragm, and was used for gating with a 5 mm gating window. A free-breathing single-shot ECG-triggered bSSFP sequence with the following parameters was used for the acquisition of the mid-ventricular short-axis slice: 2D single-slice, FOV = 320×320 mm^2, in-plane resolution = 2.5×2.5 mm^2, slice thickness = 8 mm, TR/TE = 2.7 ms/1.35 ms, flip angle = 85°, 10 linear ramp-up pulses, SENSE rate = 2, acquisition window = 181 ms, number of phase encoding lines = 67, linear k-space ordering. All acquisitions were performed with 27 images corresponding to different T_2prep echo times, including TE_{T2P} = 0 and TE_{T2P} ranging from 25 ms to 150 ms in steps of 5 ms. An additional SAT image was also acquired for the 3-parameter fit. T_2 maps were also generated for the short acquisition configurations. The nominal scan time for these scans, acquiring all 27 T_2prep echoes, was 3:10 minutes at 60 heart-beats per min, assuming 100% NAV gating efficiency.

T_2 Map Analysis—The acquired images were registered retrospectively using an advanced non-rigid image registration algorithm (32) to compensate for residual in-slice motion. This algorithm simultaneously estimates a non-rigid motion field and intensity variations, and employs an additional regularization term to constrain the deformation field using automatic feature tracking. Voxel-wise curve-fitting was performed, subsequent to registration, to generate T_2 maps for the 3-parameter and the 2-parameter models. T_2 maps were generated for different subsets of images corresponding to different T_2prep echo times, as described for phantom imaging. Epi- and endocardial contours were drawn manually by an experienced blinded reader for each T_2 map. The average T_2 value and the standard deviation within the septum were recorded.

Finally, a segment-based analysis was performed for the proposed 3-parameter model with the SAT images. Variations in T_2 and B/A across different segments were studied to see if the regional variations were due to tissue characteristics or due to sequence parameters, as described by Equation [6]. 6 segments were used in the mid-ventricular LV slice, in accordance with the AHA 16-segment model (33). Segment-based T_2 and B/A values were recorded for each subject. These were then averaged over all subjects for each segment. The B/A value was also compared to the value predicted by Equation [6] for the given sequence parameters.

Results

Numerical Simulations

Figure 2 shows the effect of B_0 and B_1 variations on T_2 estimation. Figure 2(a) shows the normalized longitudinal magnetization measured directly after the T_2prep sequence. Figure 2(b-d) shows the errors in T_2 estimation using 2-parameter fit, and 3-parameter fit, with and without the proposed compensation of 90°, -90° pulses for $TE_{T2P} = 0$. The green area in Figure 2(b) shows valid T_2 estimations (within ±5ms) over a ΔB_0 range of ±200 Hz and a ΔB_1 range of 20%. Using the 3-parameter fit in Figure 2(d) reduced the B_0 range to around ±150 Hz but increased the B_1 range to nearly 30%. However, when the proposed 90°, -90° was used for $TE_{T2P} = 0$, the B_0 range to increased to almost 250 Hz with the same B_1 range (Figure 2(e)). This was not the case with the 2-parameter fit in Figure 2(c) where a bias of 10-30 ms was observed in the estimated T_2 values for almost the whole range of B_0-B_1 variations.

Phantom Imaging

3-parameter vs. 2-parameter Fit—Figure 3 shows the accuracy and precision of the three different fitting approaches (2-parameter, 3-parameter without SAT image and the proposed 3-parameter with SAT image) on various subsets of images corresponding to different T_2prep echo times for a vial with a T_2 value of 47 ms. The red, green, blue, purple and black points correspond to $TE_{T2P} = 0$ and n TE_{T2P} values starting from 25 ms in steps of 5, 10, 15, 20 and 25 ms respectively, and the value of n is depicted on the horizontal axis. The T_2 value estimated with the 2-parameter model increased with the number of T_2prep echoes. For example, a 2-parameter fit on 9 T_2prep echoes resulted in an estimated T_2 value of 64 ms, as opposed to an estimate of 55 ms for 5 T_2prep echoes, when a 10 ms TE_{T2P} spacing was used. The echo spacing also affected the estimated T_2 value for the 2-parameter model. For example, using 7 T_2prep echo times, a 5 ms TE_{T2P} spacing led to a 55 ms T_2 estimate, whereas a 25 ms TE_{T2P} spacing resulted in the estimation of 63 ms as the T_2 value. These exemplify the mismatch between the acquisition and the 2-parameter model. The 3-parameter fit without SAT image converged to the T_2 value after 7 T_2prep echoes. However, if the number of T_2prep echoes was not sufficient, it overestimated the T_2 value, with a high level of noise as apparent in the precision measurements. The T_2 value estimated using the 3-parameter fit with the SAT image remained almost constant (variation: 2 ms) for different subsets of T_2prep echo times. Figure 4 shows examples of the fit for the short acquisition and for 27 T_2prep echoes, for the same vial, where the signal in the ROI is averaged prior to fitting. The overestimation of the T_2 value using 3 T_2prep echoes and the 2-parameter fit were visualized in the under-estimation of the non-zero signal value corresponding to the long T_2prep echo time ("T_2prep = ∞"). When using 27 echoes, the 3-parameter fit without SAT image matched the behavior of the proposed 3-parameter fit with SAT image, while the 2-parameter fit still overestimated the T_2 values.

Figure 5 depicts the correlation of the different T_2 curve fitting methods using the short acquisition or all 27 T_2prep echoes, with respect to the spin echo sequence. The proposed 3-parameter fit with SAT image, using the short acquisition or all 27 T_2prep echoes, produced T_2 values that were not significantly different than the reference values generated using a

spin echo acquisition ($P = 0.104$ and 0.3, respectively). The 3-parameter fit without SAT image showed no significant differences for both the short acquisition and 27 T_2prep echoes ($P = 0.073$ and 0.126 respectively). The conventional 2-parameter fit significantly overestimated the T_2 values for both 3 and 27 T_2prep echoes ($P = 0.013$ and 0.005, respectively).

Effect of the B_1 inhomogeneities—The T_2 values using the proposed 3-parameter fit with SAT image were not significantly different than the spin echo values, as described above, when using the proposed RF compensation ($P = 0.3$). However, the difference was significant without the compensation ($P < 0.001$). The 2-parameter fit led to significant differences in T_2 values, both with and without the compensation ($P = 0.005$ and 0.010 respectively).

Length of the Rest Cycles—Figure 6 shows the effect of the length of rest cycles. The error in the estimated T_2 was the highest for vials with long T_1 values due to insufficient magnetization recovery. This error gradually decreased with increasing rest cycles. For the vials with T_1 and T_2 ranges near the myocardium and for rest cycles ≥ 4s, the error was within 2 ms and 1 ms when using the short acquisition and 27 samples, respectively.

In Vivo Imaging

The myocardial T_2 mapping sequence was successfully completely in all subjects without complications. The average scan time to acquire all 27 echoes was 3:30 ± 0:10 minutes (range: 3:17 to 3:47 minutes). The difference between the nominal scan time and the actual average scan time is due to the differences in breathing patterns and heart rates of the subjects. Figure 7 shows example T_2 maps from a healthy subject, generated using the three different fitting approaches (2-parameter, 3-parameter without SAT image and the proposed 3-parameter with SAT image) with the short acquisition, as well as all 27 T_2prep echoes. The myocardial T_2 value for the 2-parameter fit increased when using 27 T_2prep echoes instead of 3, which was consistent with phantom imaging. For the short acquisitions, the T_2 map generated using the 3-parameter fit without SAT image visibly showed more signal inhomogeneity compared to that of the proposed 3-parameter fit with SAT. The quality of the T_2 map for the 3-parameter fit without SAT image improved with 27 T_2prep echoes. The proposed 3-parameter fit with SAT image led to similar quality myocardial T_2 maps with 3 and 27 echoes.

Figure 8 shows the estimated T_2 values (averaged over an ROI in the septum) from the same subject in Figure 7 using the three fitting methods (2-parameter, 3-parameter without SAT image and the proposed 3-parameter with SAT image) on various subsets of images corresponding to different T_2prep echo times. Similar to phantom imaging, the T_2 value estimated with the 2-parameter fitting method increased with increasing number of T_2prep echo times. The T_2 value estimated using the 3-parameter fit without SAT image showed a convergence trend with increased number of T_2prep echo times. The proposed 3-parameter fitting with SAT image yielded T_2 values which are independent of number of T_2prep echoes. The standard deviation of T_2 values in the ROI decreased with higher number of echoes for all fitting methods.

Table 1 summarizes the ventricular septum T_2 values for all of the healthy adult subjects using the three fitting methods, and the short acquisition or 27 T_2prep echoes. The maximum variation (among all subjects) of the myocardial T_2 values between using 3 or 27 T_2prep echoes, was 3.7 ms with the proposed 3-parameter fitting with SAT image. The range of increase in the T_2 values, among all subjects, was 4.6 - 20.0 ms when the 2-parameter fit is used with 27 T_2prep echoes instead of 3 T_2prep echoes. T_2 measurements could not be performed on two maps generated using the 3-parameter fitting without SAT image and the short acquisition due to the high levels of inhomogeneity in the myocardium. Furthermore, for the T_2 maps from the short acquisitions where measurements could be performed, the precision of the 3-parameter fit with the SAT image was significantly better than that of the 3-parameter fit without the SAT image (8.5 ± 2.1 ms vs. 15.5 ± 5.1 ms, $P = 0.009$).

Table 2 depicts the results of the segment-based analysis for the proposed 3-parameter fit with 27 echoes. The range variation for the average T_2 values across the six segments is 4.2 ms (between 52.6 and 56.8 ms), showing less than 10% variation. The range of variation for the B/A values is 0.01, with a mean value of 0.14 or 0.15 across all segments. The B/A value predicted by Equation [6] for these sequence parameters is 0.13 (with T_1 = 1200 ms and T_2 = 55 ms), which is consistent with the experimental findings.

Discussion

In this study, we proposed a 3-parameter model for T_2 relaxation to characterize T_2-prepared bSSFP acquisitions. For efficient estimation of these three parameters, we also proposed a novel sequence that incorporates saturation-prepared images in addition to T_2-prepared images, as well as an efficient navigator-gating scheme for free-breathing acquisitions. This new sequence and the 3-parameter model improve the accuracy of myocardial T_2 mapping.

The 3-parameter model for curve-fitting was found to be independent of the choice of T_2prep echo times, whereas the estimated T_2 values changed with T_2prep echo times using the 2-parameter model. Since the 2-parameter model does not take into account the disturbance in magnetization due to the startup and imaging pulses until the acquisition of central k-space, this leads to a model mismatch between the curve-fitting and the underlying acquisition, which makes the estimated T_2 value a function of the T_2prep echo times. This model mismatch is resolved using the 3-parameter model, and the dependence of the estimated T_2 value on where the T_2 relaxation curve is sampled is eliminated.

Apart from its independence from the sequence parameters, the 3-parameter model with the SAT image is accurate with respect to the spin echo sequence, after the proposed modifications to account for RF pulse imperfection. The inaccuracy of T_2 mapping procedure with the 2-parameter curve-fitting with respect to the spin echo sequence, as well as its dependence on k-space profile ordering, has been noted previously (11). However, this discrepancy was not examined further in (11).

The reference T_2 maps with CPMG spin echo sequence were generated with a 2-parameter fit. The issue of magnetization disturbance due to imaging pulses in single shot sequences is

not present for this acquisition, thus a 2-parameter fit is appropriate. The 3-parameter fit for the spin echo acquisition (not shown) also yields the same values.

We chose to acquire 27 images with different T_2prep echo times in each scan for this study. This was done to study the effect of different choices of T_2prep times on the overall estimation procedure using the 3-parameter and 2-parameter models. This number of echoes is not required for attaining accuracy and precision for in-vivo imaging using the proposed 3-parameter curve fitting with the additional SAT image. Furthermore, the precision gain going from 3 echoes to 27 echoes is at most 4.3 ms for the myocardium in this technique.

In (28), it was concluded that the 3-parameter fit cannot be robustly used with 4 finite T_2prep echoes. However, our experience indicates that 3 T_2prep echoes of 0, 25, 50 ms, and an additional SAT image are sufficient to provide accurate and precise T_2 maps. Using 6 second rest cycles, this exam can be completed in 16 seconds at 60 bpm heart-rate, which is attainable with a breath-hold acquisition. The improvement in our sequence in terms of robustness with a small number of T_2prep echoes comes from the use of the SAT image instead of a large T_2prep echo time, which significantly improves the precision in-vivo. Compared to the sampling of a large T_2prep echo time, such as 90 ms, the SAT image (equivalently T_2prep echo time ∞) enables direct estimation of the B parameter in Equation [2], and higher quality estimates of T_2 values. Furthermore, in Appendix A, we analytically show that from an estimation theoretic perspective, sampling the SAT image is more beneficial in terms of precision of T_2 maps in the presence of noise compared to sampling a large but finite T_2prep echo time. Another benefit of using the SAT image is that it can be acquired without any preceding rest periods, whereas a 6 second rest period would be necessary to acquire a large T_2prep echo time.

The segment-based analysis of the B/A parameter from the fitting procedure leads to values which are consistent with the theoretical predictions. The minor pixel-dependent differences may be due to the least squares fitting procedure, which approximates the Rician noise in the images as Gaussian noise with a non-zero mean (34), which would be reflected in the B parameter. Due to this good correspondence, between theory as predicted in Equation [6] and the experimental results, the utility of the B term is expected to extend to different phase encode schemes. Small regional variations of the T_2 values were also observed.

For both the SAT image and for images acquired with large T_2prep echo times, the underlying SNR may be too low to approximate the Rician noise as Gaussian noise, which is implicitly done in the least squares estimation process. This may cause a bias in the estimation procedure. However, this was not observed in our phantom experiments. Nonetheless, it might be beneficial to acquire multiple SAT images, since no rest cycles are required between them, and average them prior to fitting to further mitigate any bias.

Apart from the use of SAT images instead of large T_2prep echo times, optimal selection of T_2prep echo times to further improve robustness was not explored experimentally. In Appendix A, an estimation theoretic analysis to maximize the precision of the T_2 maps shows that it would be beneficial to choose a tri-modal distribution of T_2prep echo times, with the points concentrating at 0 ms, at an echo time near the T_2 value of interest and at ∞,

with the multiplicity changing based on the total number of echoes. However, in our experiments, we used a more standard distribution of T_2prep echo times based on the existing literature. Further experiments are warranted to systematically optimize the T_2prep echo time distribution, but this is not the focus of the current work.

A new navigator-gating scheme was proposed to improve the efficiency for free-breathing acquisitions. In the conventional scheme proposed in (35), the T_2prep follows the NAV signal, however it is performed regardless of the position of the NAV signal, necessitating additional rest periods if the NAV signal is outside the gating window. In our proposed approach, the T_2prep is conditionally applied based on the position of the NAV signal. Thus, if the NAV signal is outside the gating window, no preparation or imaging pulses are applied, and the magnetization remains undisturbed. This also eliminates the necessity for rest periods if the NAV signal is outside the gating window. Thus, the overall efficiency of the acquisition is improved.

Since the NAV signal is placed before the T_2 preparation, there is a longer separation between the image acquisition and the NAV signal. This may lead to residual motion in the images, necessitating image registration to mitigate residual motion artifacts. The efficacy of the particular image registration algorithm in T_2 mapping was not systematically studied in this study, and is beyond the scope and focus of this work.

A 6 second rest period was used to allow for a full magnetization recovery between subsequent T_2prep modules. This choice was based on a $5\times T_1$ approximation, using reported myocardial T_1 values in the literature. While a 6 second rest period was used in this study to ensure sufficient recovery, phantom results indicated that 4 seconds may be sufficient, reducing the breath-hold duration for an acquisition with 3 T_2prep echoes and a SAT image. Although shorter rest periods are desirable, phantom results showed arbitrary, T_1-dependent biases in the estimated T_2 values when shorter durations were used.

This study has several limitations. Only a small number of healthy subjects were recruited. Further clinical evaluations on larger cohorts are warranted to quantify changes in T_2 relaxation times in different populations. No validation of the T_2 values has been performed in vivo, since a reference T_2 time cannot be assessed in the myocardium in a reasonable scan time. The intra-patient reproducibility of the T_2 values was also not studied. We have only considered single-shot sequences with linear ordering. The effect of including the third parameter on accuracy may be less for centric ordering or multi-shot sequences. Only a single mid-ventricular short-axis slice was imaged in this study. The low in-plane resolution used in this study may lead to partial imaging artifacts if more apical slices are acquired.

Conclusion

We propose a 3-parameter model for T_2 relaxation accurately models myocardial T_2 mapping using T_2-prepared bSSFP acquisitions. This model exhibits no dependency on the choice of T_2prep echo times, whereas such dependence is observed if a conventional 2-parameter model is used for curve-fitting. The proposed sequence incorporates SAT images in addition to T_2-prepared images, and the improved navigator-gating technique augments

the efficiency of the myocardial T_2 mapping acquisition, allowing for accurate and precise T_2 maps.

Acknowledgments

The project described was partially supported by NIH R01EB008743-01A2, NIH K99HL111410-01 and Samsung Electronics, Suwon, South Korea.

The authors thank Warren J. Manning for his editorial comments.

Appendix A

We use the Cramér-Rao Bound (CRB) to provide a lower bound on the precision of an unbiased T_2 estimator, and subsequently minimize this bound numerically to find the optimal selection of T_2prep echo times, similar to the approaches in (36,37). For the model in Equation [7] with least squares estimation of T_2, and for K T_2prep echo times, $\{x_1, x_2, \ldots, x_k\}$, the Fisher information matrix is given by

$$\mathbf{I} = \begin{bmatrix} \sum_{k=1}^{K} \left(e^{\frac{-x_k}{T_2}} \right)^2 & \sum_{k=1}^{K} e^{\frac{-x_k}{T_2}} & \sum_{k=1}^{K} Ae^{\frac{-x_k}{T_2}} \frac{x_k}{T_2^2} \\ \sum_{k=1}^{K} e^{\frac{-x_k}{T_2}} & \sum_{k=1}^{K} (1)^2 & \sum_{k=1}^{K} Ae^{\frac{-x_k}{T_2}} \frac{x_k}{T_2^2} \\ \sum_{k=1}^{K} Ae^{\frac{-x_k}{T_2}} \frac{x_k}{T_2^2} & \sum_{k=1}^{K} Ae^{\frac{-x_k}{T_2}} \frac{x_k}{T_2^2} & \sum_{k=1}^{K} \left(Ae^{\frac{-xk}{T_2}} \frac{x_k}{T_2^2} \right)^2 \end{bmatrix}. \quad [A1]$$

The CRB on the variance of the T_2 estimate is given by

$$\begin{aligned} \mathrm{var}\left(\hat{T}_2\right) &\geq J\left(A, T_2, \{x_k\}\right) = \left[\mathbf{I}^{-1}\right]_{3,3} \quad [A2] \\ &= \frac{\mathbf{I}_{11}\mathbf{I}_{22} - \mathbf{I}_{12}^2}{\mathbf{I}_{11}\left(\mathbf{I}_{22}\mathbf{I}_{33} - \mathbf{I}_{23}^2\right) - \mathbf{I}_{12}\left(\mathbf{I}_{33}\mathbf{I}_{12} - \mathbf{I}_{23}\mathbf{I}_{13}\right) + \mathbf{I}_{13}\left(\mathbf{I}_{12}\mathbf{I}_{23} - \mathbf{I}_{22}\mathbf{I}_{13}\right)}, \end{aligned}$$

where $\mathbf{I}_{ij}$ denotes the $(i,j)^{\text{th}}$ entry of $\mathbf{I}$. To find the selection of T_2prep echo times that minimizes the variance of the error, we propose to solve

$$\left\{x_k^{samp}\right\} = \arg \min_{\{x_k\}} J\left(A, T_2, \{x_k\}\right) \quad [A3]$$

for a given range of T_2 values of interest. We also note that $J(A, T_2, \{x_k\})$ scales with $1/A^2$, and thus $J(A, T_2, \{x_k\}) = J(1, T_2, \{x_k\})/A^2$, and hence the selection of T_2prep echo times does not depend on A or B, but only on the T_2 values of interest.

$J(1, T_2, \{x_k\})$ was numerically minimized for T_2 values of interest from 45 ms to 60 ms, for $K = 4$ and $K = 28$. For $K = 4$, this yielded a tri-modal distribution with T_2prep echo times of 0, 49 ms (sampled twice) and ∞. For $K = 28$, the distribution of T_2prep echo times of 0 (sampled six times), 53 ms (sampled fourteen times) and ∞ (sampled 8 times). This kind of tri-modal distribution is consistent with the bi-modal distribution in (36) for the 2-parameter T_2 model, and the tri-modal one in (37) for the 3-parameter T_1 model.

Furthermore, if instead of the ∞ T_2prep echo time, one could only sample a maximum finite value of 90 ms, the distributions changed to 0, 32 ms (sampled twice) and 90 ms for $K = 4$; and 0 (sampled six times), 33 ms (sampled fourteen times) and 90 (sampled 8 times) for $K = 28$. In this case, the variance of the T_2 estimate increased by 5.4-fold and 5.5-fold for $K = 4$ and 28, respectively. A direct comparison for $K = 4$ also showed that T_2prep echo times {0, 25, 50, 90} had 5.6-fold higher variance compared to {0, 25, 50, ∞}. These results indicate that sampling the ∞ T_2prep echo time improves the precision of the fit compared to sampling a large but finite T_2prep echo time.

We note that this derivation is based on the least squares estimation, which has a one-to-one correspondence with a Gaussian noise model in the images. However, the noise in the magnitude images is Rician, which can be well-approximated by Gaussian noise for images with sufficient SNR (34), and assumption that may not hold for I_{SAT} images. This may lead to a model mismatch and an apparent bias in T_2 estimates, although this was not observed in our study.

References

1. Abdel-Aty H, Zagrosek A, Schulz-Menger J, Taylor AJ, Messroghli D, Kumar A, Gross M, Dietz R, Friedrich MG. Delayed enhancement and T2-weighted cardiovascular magnetic resonance imaging differentiate acute from chronic myocardial infarction. Circulation. 2004; 109(20):2411–2416. [PubMed: 15123531]
2. Cury RC, Shash K, Nagurney JT, Rosito G, Shapiro MD, Nomura CH, Abbara S, Bamberg F, Ferencik M, Schmidt EJ, Brown DF, Hoffmann U, Brady TJ. Cardiac magnetic resonance with T2-weighted imaging improves detection of patients with acute coronary syndrome in the emergency department. Circulation. 2008; 118(8):837–844. [PubMed: 18678772]
3. Raman SV, Simonetti OP, Winner MW 3rd, Dickerson JA, He X, Mazzaferri EL Jr, Ambrosio G. Cardiac magnetic resonance with edema imaging identifies myocardium at risk and predicts worse outcome in patients with non-ST-segment elevation acute coronary syndrome. J Am Coll Cardiol. 2010; 55(22):2480–2488. [PubMed: 20510215]
4. Friedrich MG, Sechtem U, Schulz-Menger J, Holmvang G, Alakija P, Cooper LT, White JA, Abdel-Aty H, Gutberlet M, Prasad S, Aletras A, Laissy JP, Paterson I, Filipchuk NG, Kumar A,

Pauschinger M, Liu P. Cardiovascular magnetic resonance in myocarditis: A JACC White Paper. J Am Coll Cardiol. 2009; 53(17):1475–1487. [PubMed: 19389557]

5. Abdel-Aty H, Boye P, Zagrosek A, Wassmuth R, Kumar A, Messroghli D, Bock P, Dietz R, Friedrich MG, Schulz-Menger J. Diagnostic performance of cardiovascular magnetic resonance in patients with suspected acute myocarditis: comparison of different approaches. J Am Coll Cardiol. 2005; 45(11):1815–1822. [PubMed: 15936612]
6. Butler CR, Thompson R, Haykowsky M, Toma M, Paterson I. Cardiovascular magnetic resonance in the diagnosis of acute heart transplant rejection: a review. J Cardiovasc Magn Reson. 2009; 11:7. [PubMed: 19284612]
7. Abdel-Aty H, Cocker M, Friedrich MG. Myocardial edema is a feature of Tako-Tsubo cardiomyopathy and is related to the severity of systolic dysfunction: insights from T2-weighted cardiovascular magnetic resonance. Int J Cardiol. 2009; 132(2):291–293. [PubMed: 18086501]
8. Simonetti OP, Finn JP, White RD, Laub G, Henry DA. “Black blood” T2-weighted inversion-recovery MR imaging of the heart. Radiology. 1996; 199(1):49–57. [PubMed: 8633172]
9. Abdel-Aty H, Simonetti O, Friedrich MG. T2-weighted cardiovascular magnetic resonance imaging. J Magn Reson Imaging. 2007; 26(3):452–459. [PubMed: 17729358]
10. Arai AE. Using magnetic resonance imaging to characterize recent myocardial injury: utility in acute coronary syndrome and other clinical scenarios. Circulation. 2008; 118(8):795–796. [PubMed: 18711021]
11. Giri S, Chung YC, Merchant A, Mihai G, Rajagopalan S, Raman SV, Simonetti OP. T2 quantification for improved detection of myocardial edema. J Cardiovasc Magn Reson. 2009; 11:56. [PubMed: 20042111]
12. McNamara MT, Higgins CB, Schechtmann N, Botvinick E, Lipton MJ, Chatterjee K, Amparo EG. Detection and characterization of acute myocardial infarction in man with use of gated magnetic resonance. Circulation. 1985; 71(4):717–724. [PubMed: 3971541]
13. Bottomley PA, Foster TH, Argersinger RE, Pfeifer LM. A review of normal tissue hydrogen NMR relaxation times and relaxation mechanisms from 1-100 MHz: dependence on tissue type, NMR frequency, temperature, species, excision, and age. Med Phys. 1984; 11(4):425–448. [PubMed: 6482839]
14. He T, Gatehouse PD, Anderson LJ, Tanner M, Keegan J, Pennell DJ, Firmin DN. Development of a novel optimized breathhold technique for myocardial T2 measurement in thalassemia. J Magn Reson Imaging. 2006; 24(3):580–585. [PubMed: 16892203]
15. Foltz WD, Stainsby JA, Wright GA. T2 accuracy on a whole-body imager. Magn Reson Med. 1997; 38(5):759–768. [PubMed: 9358450]
16. Blume U, Lockie T, Stehning C, Sinclair S, Uribe S, Razavi R, Schaeffter T. Interleaved T(1) and T(2) relaxation time mapping for cardiac applications. J Magn Reson Imaging. 2009; 29(2):480–487. [PubMed: 19161206]
17. van Heeswijk RB, Feliciano H, Bongard C, Bonanno G, Coppo S, Lauriers N, Locca D, Schwitter J, Stuber M. Free-breathing 3 T magnetic resonance T2-mapping of the heart. JACC Cardiovasc Imaging. 2012; 5(12):1231–1239. [PubMed: 23236973]
18. Verhaert D, Thavendiranathan P, Giri S, Mihai G, Rajagopalan S, Simonetti OP, Raman SV. Direct T2 quantification of myocardial edema in acute ischemic injury. JACC Cardiovasc Imaging. 2011; 4(3):269–278. [PubMed: 21414575]
19. Zia MI, Ghugre NR, Connelly KA, Strauss BH, Sparkes JD, Dick AJ, Wright GA. Characterizing myocardial edema and hemorrhage using quantitative T2 and T2* mapping at multiple time intervals post ST-segment elevation myocardial infarction. Circ Cardiovasc Imaging. 2012; 5(5): 566–572. [PubMed: 22744938]
20. Foltz WD, Al-Kwifi O, Sussman MS, Stainsby JA, Wright GA. Optimized spiral imaging for measurement of myocardial T2 relaxation. Magn Reson Med. 2003; 49(6):1089–1097. [PubMed: 12768587]
21. Brittain JH, Hu BS, Wright GA, Meyer CH, Macovski A, Nishimura DG. Coronary angiography with magnetization-prepared T2 contrast. Magn Reson Med. 1995; 33(5):689–696. [PubMed: 7596274]

22. Huang TY, Liu YJ, Stemmer A, Poncelet BP. T2 measurement of the human myocardium using a T2-prepared transient-state TrueFISP sequence. Magn Reson Med. 2007; 57(5):960–966. [PubMed: 17457877]

23. Foltz WD, Yang Y, Graham JJ, Detsky JS, Dick AJ, Wright GA. T2 fluctuations in ischemic and post-ischemic viable porcine myocardium in vivo. J Cardiovasc Magn Reson. 2006; 8(3):469–474. [PubMed: 16755833]

24. Park CH, Choi EY, Kwon HM, Hong BK, Lee BK, Yoon YW, Min PK, Greiser A, Paek MY, Yu W, Sung YM, Hwang SH, Hong YJ, Kim TH. Quantitative T2 mapping for detecting myocardial edema after reperfusion of myocardial infarction: validation and comparison with T2-weighted images. Int J Cardiovasc Imaging. 2013; 29(Suppl 1):65–72. [PubMed: 23765068]

25. Usman AA, Taimen K, Wasielewski M, McDonald J, Shah S, Giri S, Cotts W, McGee E, Gordon R, Collins JD, Markl M, Carr JC. Cardiac magnetic resonance T2 mapping in the monitoring and follow-up of acute cardiac transplant rejection: a pilot study. Circ Cardiovasc Imaging. 2012; 5(6): 782–790. [PubMed: 23071145]

26. Wassmuth R, Prothmann M, Utz W, Dieringer M, von Knobelsdorff-Brenkenhoff F, Greiser A, Schulz-Menger J. Variability and homogeneity of cardiovascular magnetic resonance myocardial T2-mapping in volunteers compared to patients with edema. J Cardiovasc Magn Reson. 2013; 15:27. [PubMed: 23537111]

27. Walker PM, Marie PY, Mezeray C, Bessieres M, Escanye JM, Karcher G, Danchin N, Mattei S, Villemot JP, Bertrand A. Synchronized inversion recovery-spin echo sequences for precise in vivo T1 measurement of human myocardium: a pilot study on 22 healthy subjects. Magn Reson Med. 1993; 29(5):637–641. [PubMed: 8389415]

28. Giri, S., Chung, Y., Shah, S., Xue, H., Guehring, J., Zuehlsdorff, S., Simonetti, OP. T2 mapping using T2prepared-SSFP: optimizing echo time, flip angle and parameter fitting. 2010 May; Stockholm. Proceedings of the 18th Scientific Meeting of ISMRM; p. 2960

29. Levitt M, Freeman R, Frenkiel T. Broadband heteronuclear decoupling. J Magn Reson. 1982; 47:328–330.

30. Scheffler K. On the transient phase of balanced SSFP sequences. Magn Reson Med. 2003; 49(4): 781–783. [PubMed: 12652552]

31. Chow K, Flewitt JA, Green JD, Pagano JJ, Friedrich MG, Thompson RB. Saturation recovery single-shot acquisition (SASHA) for myocardial T1 mapping. Magn Reson Med. 2013; Epub ahead of print. doi: 10.1002/mrm.24878

32. Roujol S, Foppa M, Weingartner S, Manning WJ, Nezafat R. Adaptive registration of varying contrast-weighted images for improved tissue characterization (ARCTIC): Application to T1 mapping. Magn Reson Med. 2014; Epub ahead of print. doi: 10.1002/mrm.25270

33. Cerqueira MD, Weissman NJ, Dilsizian V, Jacobs AK, Kaul S, Laskey WK, Pennell DJ, Rumberger JA, Ryan T, Verani MS. Standardized myocardial segmentation and nomenclature for tomographic imaging of the heart. A statement for healthcare professionals from the Cardiac Imaging Committee of the Council on Clinical Cardiology of the American Heart Association. Circulation. 2002; 105(4):539–542. [PubMed: 11815441]

34. Gudbjartsson H, Patz S. The Rician distribution of noisy MRI data. Magn Reson Med. 1995; 34(6): 910–914. [PubMed: 8598820]

35. Giri S, Shah S, Xue H, Chung YC, Pennell ML, Guehring J, Zuehlsdorff S, Raman SV, Simonetti OP. Myocardial T(2) mapping with respiratory navigator and automatic nonrigid motion correction. Magn Reson Med. 2012; 68(5):1570–1578. [PubMed: 22851292]

36. Jones JA, Hodgkinson P, Barker AL, Hore PJ. Optimal sampling strategies for the measurement of spin–spin relaxation times. J Magn Res - Series B. 1996; 113:25–34.

37. Akcakaya M, Weingartner S, Roujol S, Nezafat R. On the selection of sampling points for myocardial T1 mapping. Magn Reson Med. 2014; Epub ahead of print. doi: 10.1002/mrm.25285

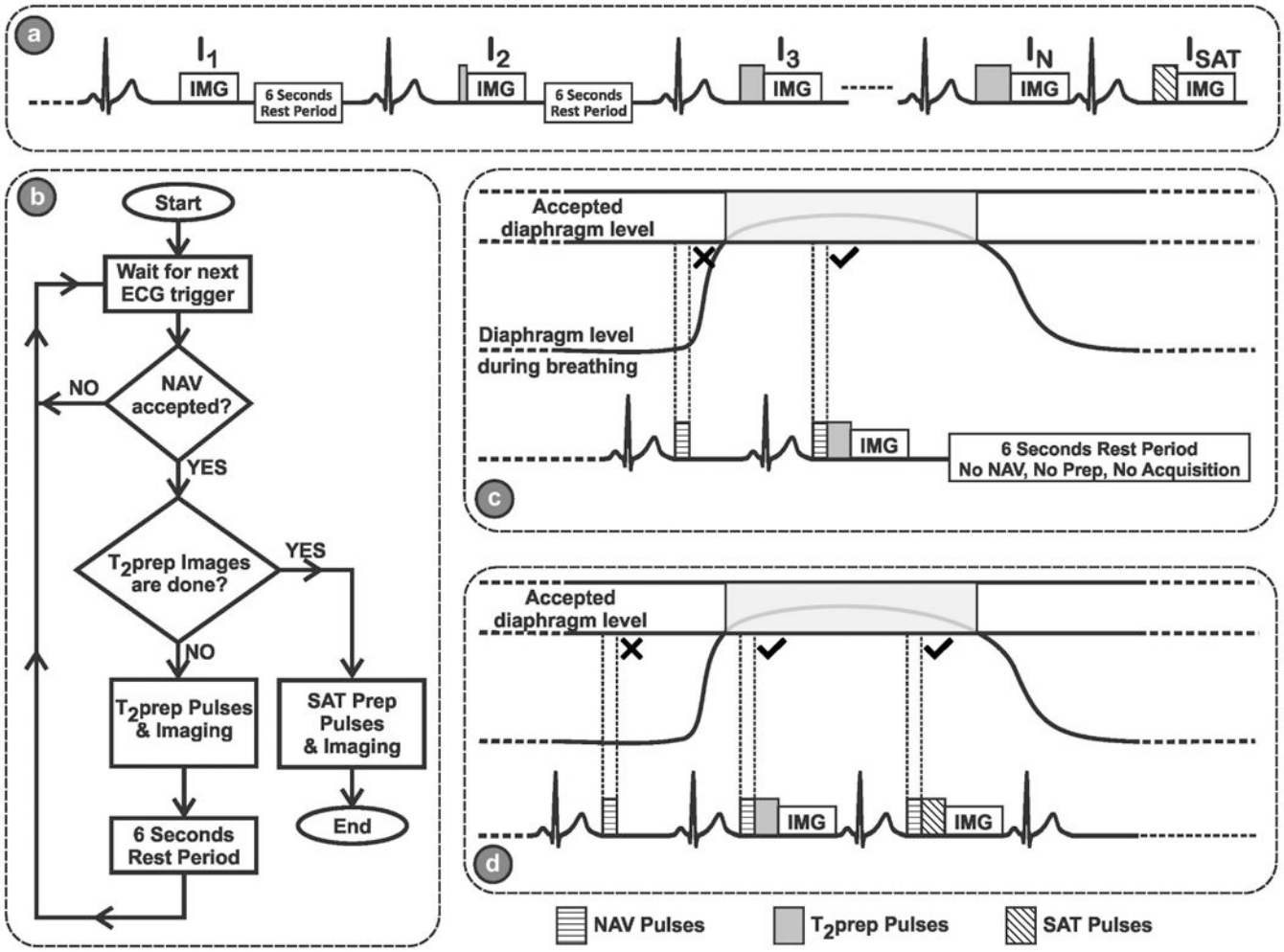

Figure 1.

(a) The schematic of the proposed sequence. Multiple single-shot images of the heart are acquired using ECG-triggering, following T_2prep of different echo lengths, TE_{T2P}. Between each image, a 6 second rest period (with no RF pulses) is applied to allow for full re-growth of the myocardium signal. An image, I_{SAT}, is acquired directly after a saturation pulse to simulate the effect of a very long T_2prep echo time (i.e. T_2prep = ∞) for improved estimation of the third parameter in the 3-parameter fit. **(b)** Flowchart for the proposed navigator (NAV)-gated acquisition scheme, The NAV is placed before the T_2prep. If the NAV signal preceding the acquisition of the k^{th} image is outside the gating window, no T_2prep or imaging pulses are applied, leaving the magnetization undisturbed, and the acquisition of this image is repeated in the next R-R interval. If the NAV signal is within the gating window, the image with the desired T_2prep time is acquired, followed by a 6 second rest period for magnetization recovery. **(c)** An example of the rejection-reacquisition scheme for a T_2-prepared image. **(d)** An example of the acquisition of a saturation-prepared image, which immediately follows the T_2-prepared image without any rest periods, and where the NAV is placed before the saturation pulse.

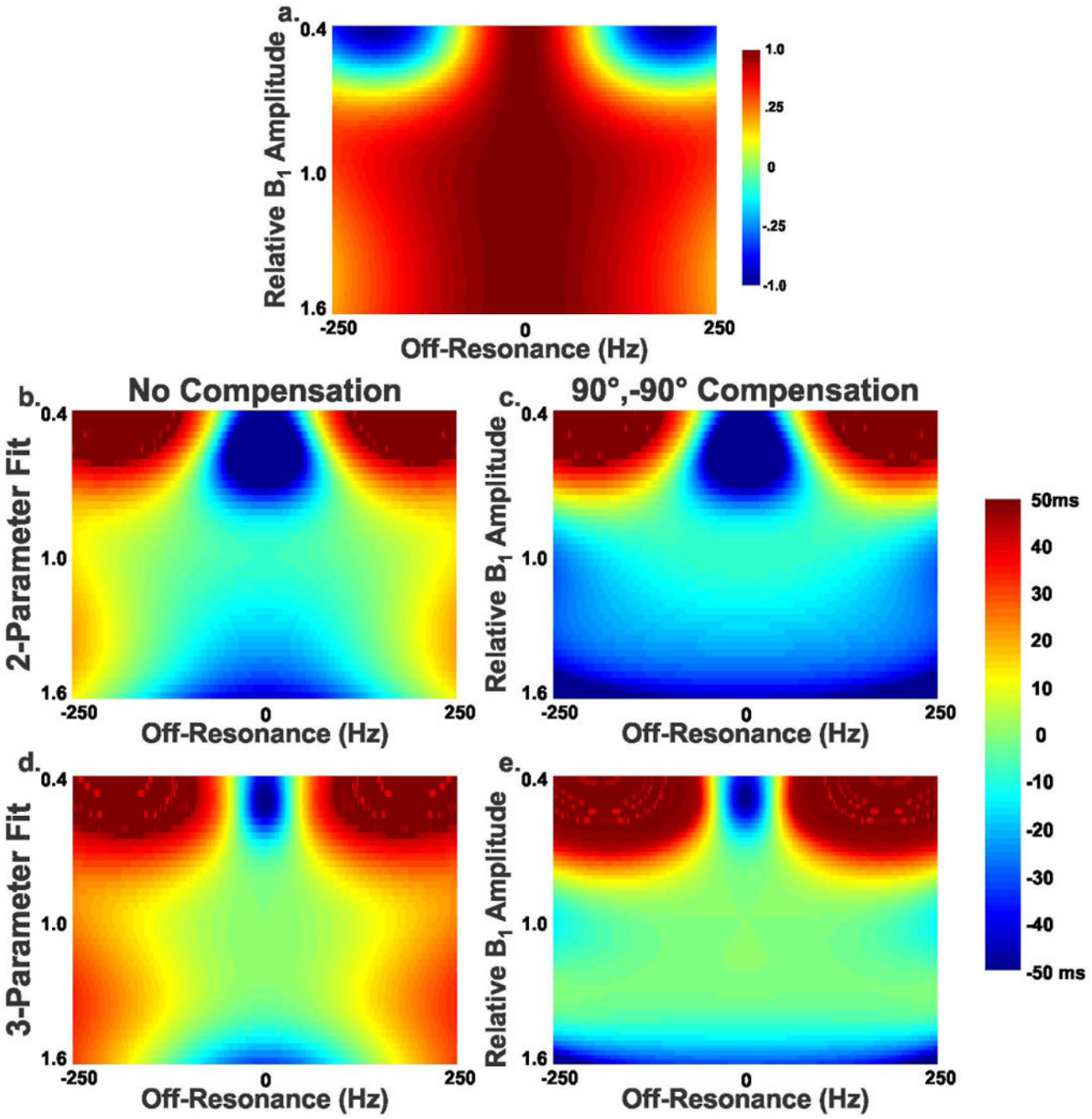

Figure 2.

Effect of B_0 and B_1 variations on T_2 estimation using simulation of Bloch equation. Nominal myocardium T_1 and T_2 values (1200 ms and 50 ms respectively) were used during simulation. The error is reported as the difference between the estimated T_2 value and the true T_2 value (50 ms). **(a)** Normalized longitudinal magnetization directly after applying the T_2prep pulse, **(b)** Error in T_2 estimation, relative to the used reference T_2 value using 2-parameter fit, **(c)** using 2-parameter fit and the proposed compensation of 90°,-90° pulses for

$TE_{T2P} = 0$, **(d)** using 3-parameter fit, and **(e)** using 3-parameter fit and the proposed compensation of 90°,-90° pulses for $TE_{T2P} = 0$.

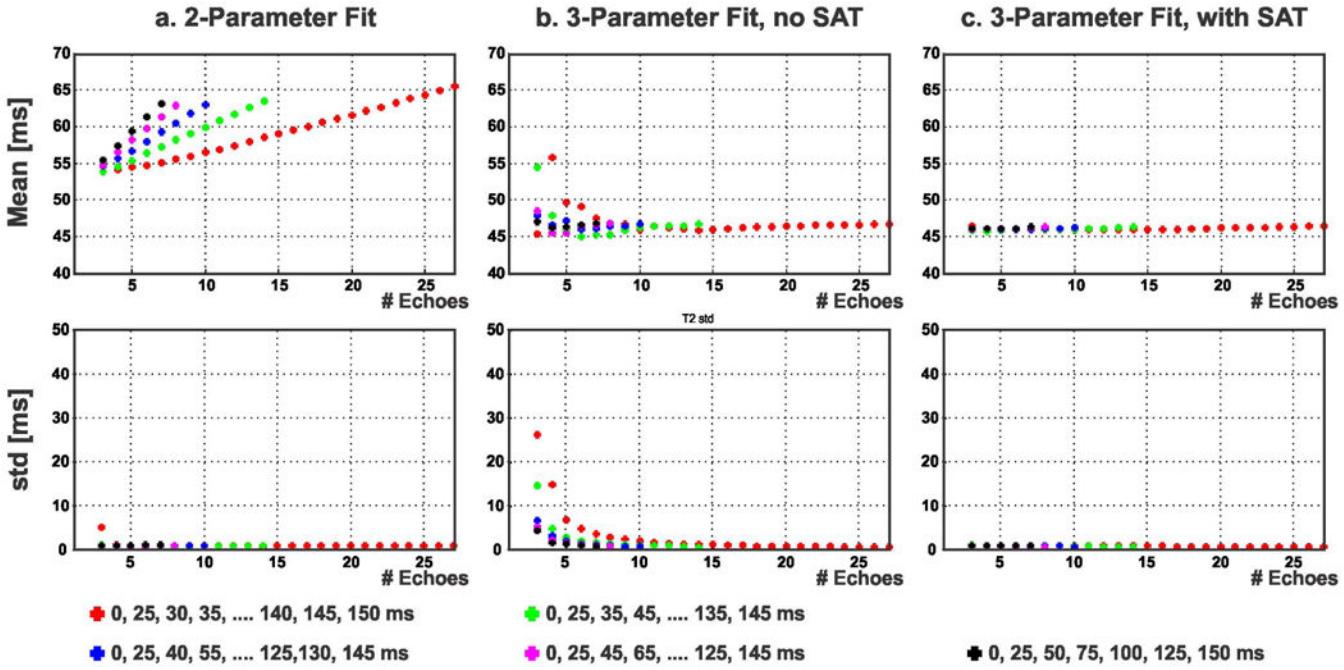

Figure 3.

Accuracy and precision of the three different fitting approaches (2-parameter, 3-parameter without saturation-prepared (SAT) image and the proposed 3-parameter with SAT image) on various subsets of images corresponding to different T_2prep echo times for a vial with a T_2 value of 47 ms. The T_2 value estimated with the 2-parameter model **(a)** shows dependence on the choice and number of T_2prep echo times. The 3-parameter fit without SAT image **(b)** showed large deviations in accuracy and precision for a small number of T_2prep echoes, but converged to the T_2 value with a large number of T_2prep echoes. The T_2 value estimated using the proposed 3-parameter fit with the SAT image **(c)** remained almost constant (variation: 2 ms) for different subsets of T_2prep echo times.

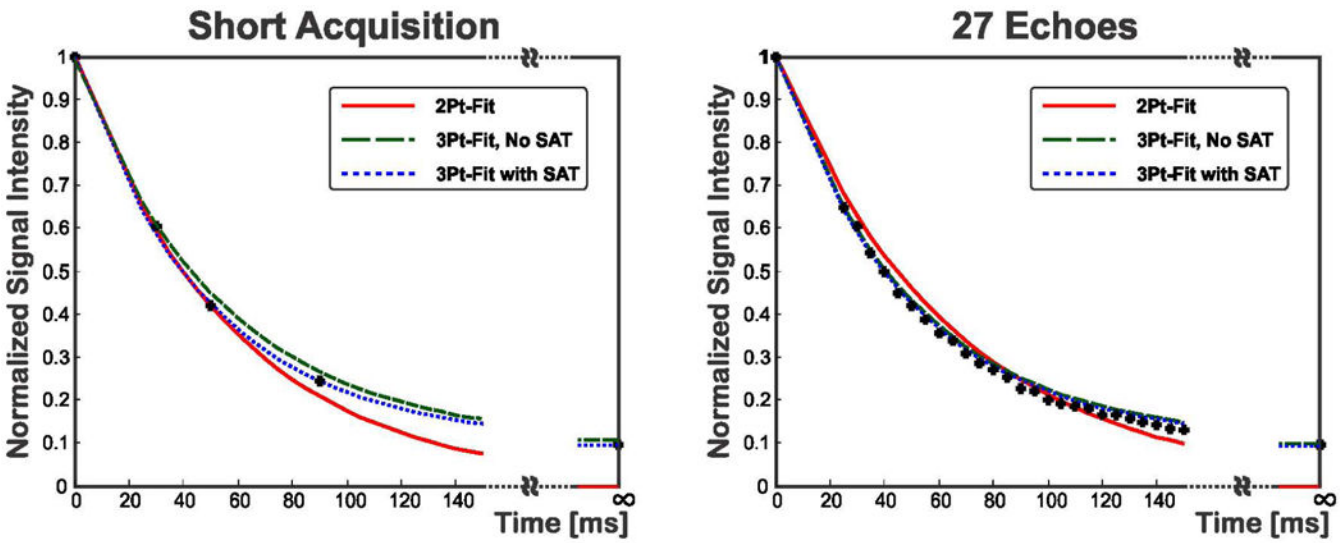

Figure 4.

Example of the fit for the short acquisition and using 27 T_2prep echoes, for the same vial in Figure 3, where the signal in the region of interest (ROI) is averaged prior to fitting. With the short acquisition, the 2-parameter overestimates the T_2 value, as apparent in the under-estimation of the non-zero signal for "T_2prep = ∞." The proposed 3-parameter fit with SAT image fits this signal value well for both 3 and 27 T_2prep echoes. With 27 echoes, the 3-parameter fit without SAT image matches the behavior of the proposed 3-parameter fit with SAT image, while the 2-parameter fit still overestimates the T_2 values.

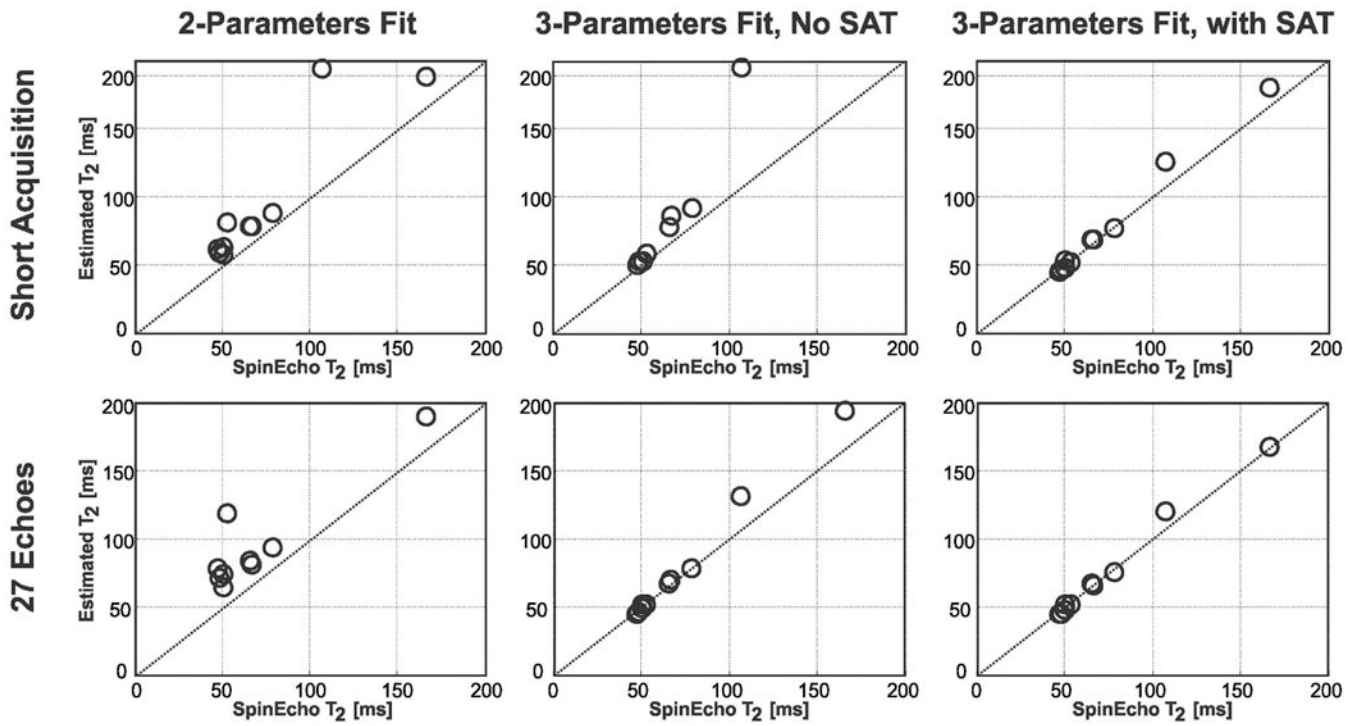

Figure 5.

T_2 values from different T_2 curve fitting methods versus the reference T_2 values generated from the spin echo sequence for all vials of the phantom, as well as the identity line. In the upper row, T_2 values are estimated using short acquisitions (i.e. 3 (0, 25, 50 ms) samples for the 2-parameter fit, 4 samples (0, 25, 50, 90 ms) for the 3-parameter fit without SAT, and 4 samples (0, 25, 50, ∞ ms) for the 3-parameter fit with SAT. In the lower row, T_2 values are estimated using long acquisitions (i.e. all 27 T_2prep echoes). The conventional 2-parameter fit significantly overestimates the T_2 values for both 3 and 27 T_2prep echoes ($P = 0.013$ and 0.005 respectively). The 3-parameter fit without SAT image results in no significant difference for either the short acquisition echoes ($P = 0.073$) or with 27 T_2prep echoes ($P = 0.126$). The proposed 3-parameter fit with SAT image, using 3 or 27 T_2prep echoes, produces T_2 values that are not significantly different than the reference values ($P = 0.104$ and 0.3 respectively).

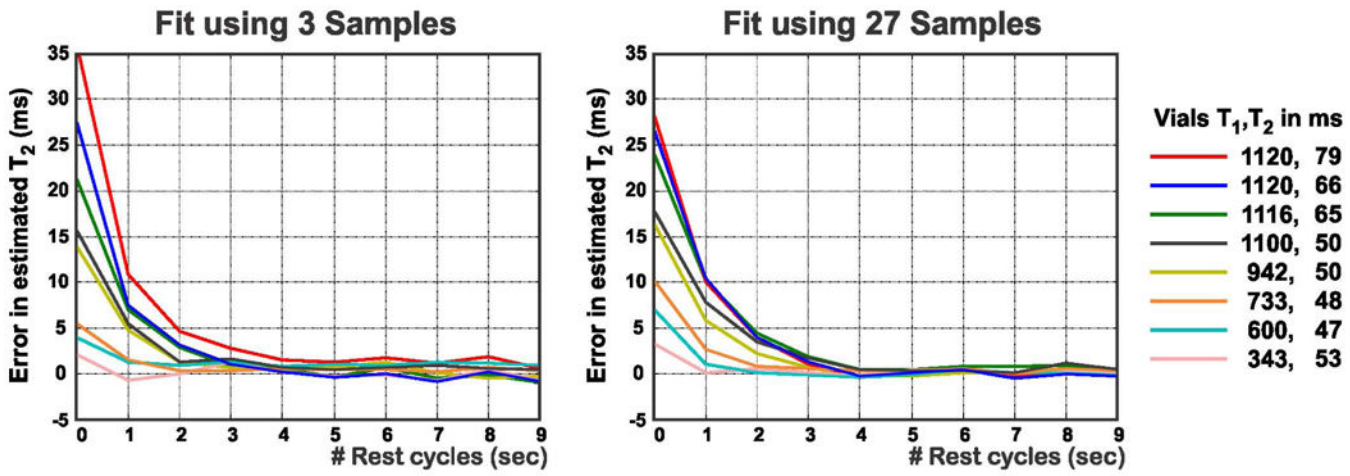

Figure 6.

Rest cycles effect on the estimated T_2 values. ROIs are placed in vials with different T_1 and T_2 values. The error is within 2 ms for both acquisitions when using rest cycles of length ≥ 4 s.

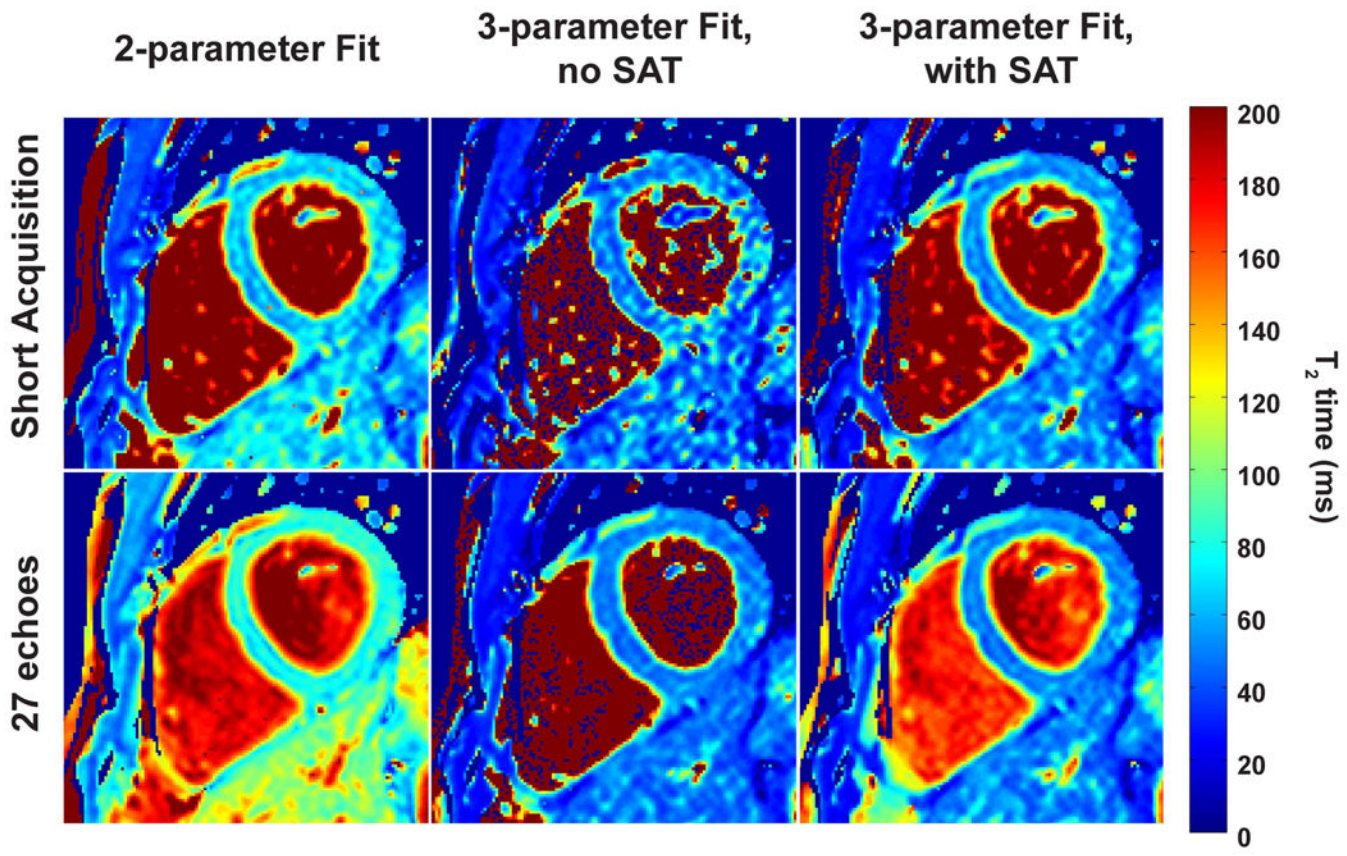

Figure 7.

Example T_2 maps from a healthy adult subject (No. 3), generated using 2-parameter fitting (left column), 3-parameter fitting without SAT image (middle column) and the proposed 3-parameter with SAT image (right column) with the short acquisition and using all 27 (top and bottom row respectively) T_2prep echoes. The myocardial T_2 value increases when going from 3 to 27 echoes using the 2-parameter fit. For the short acquisition, the T_2 map generated using the 3-parameter fit without SAT image has 1.8-fold more variation in the septum compared to that generated using the proposed 3-parameter fit with SAT image. When using all 27 T_2prep echoes, the 3-parameter fits with and without SAT image leads to similar quality in the myocardium.

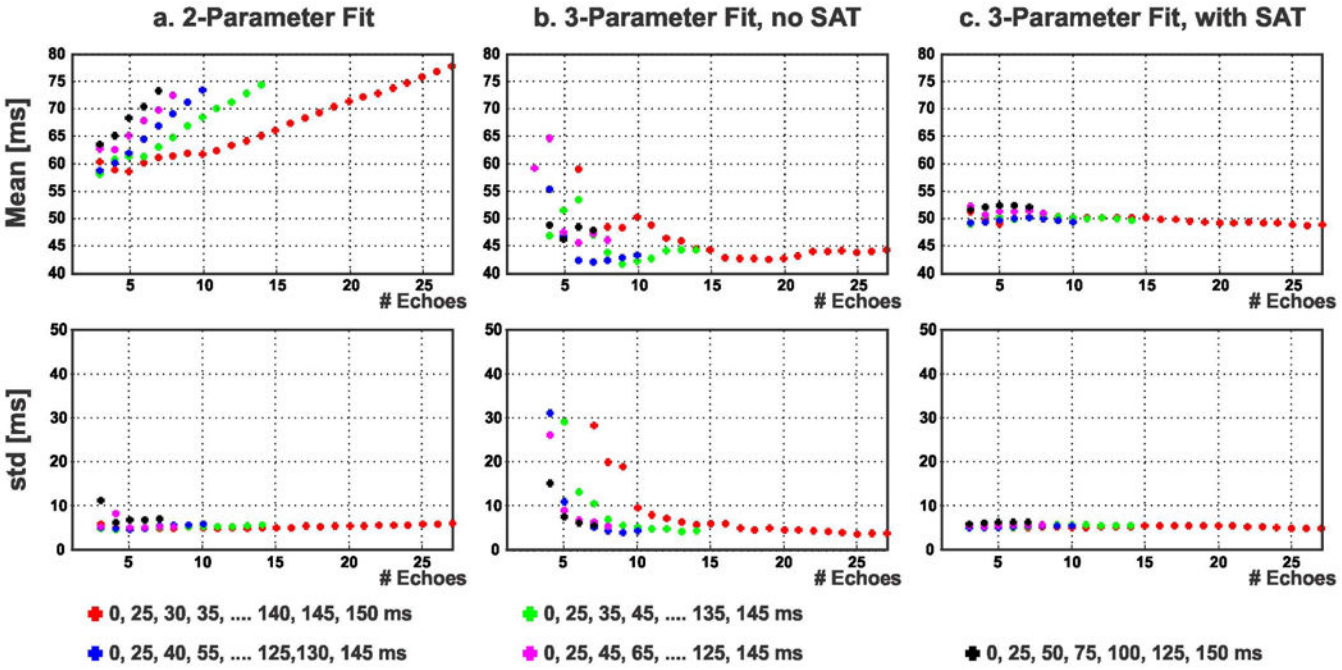

Figure 8.

Myocardial T_2 values from the same subject in Figure 7 (averaged over an ROI in the septum) using 2-parameter fit, 3-parameter fit without SAT image and the proposed 3-parameter fit with SAT image, on various subsets of image corresponding to different T_2prep echo times. The 2-parameter model **(a)** shows dependence on the choice and number of T_2prep echo times. The 3-parameter fit without SAT image **(b)** converges to the T_2 value with a large number of T_2prep echoes, but shows deviations otherwise. The proposed 3-parameter fit with the SAT image **(c)** results in T_2 values that are almost constant (variation: 3.6 ms) over different subsets of T_2prep echo times.

Table 1

Quantitative myocardial T_2 values in the ventricular septum using 2-parameter fitting, 3-parameter fitting with and without SAT image for the short acquisition and 27 T_2prep echoes. The short acquisition consists of T_2prep echoes (0 25, 50 ms) for the 2-parameter fit; (0, 25, 50, 90 ms) 3-parameter fit without SAT image; and (0 25, 50, ∞ ms) for the 3-parameter fit with SAT image.

	2-parameter Fit		3-parameter Fit, no SAT		3-parameter Fit, with SAT	
Subject	**Short Acq (ms)**	**27-echoes (ms)**	**Short Acq (ms)**	**27-echoes (ms)**	**Short Acq (ms)**	**27-echoes (ms)**
1	68.2 ± 8.0	88.2 ± 10.3	56.2 ± 12.0	49.1 ± 4.3	54.5 ± 7.0	52.4 ± 6.1
2	78.4 ± 14.3	87.3 ± 8.4	N/A	61.7 ± 8.7	62.9 ± 11.5	61.1 ± 7.2
3	63.3 ± 11.3	77.5 ± 6.1	50.3 ± 8.8	46.9 ± 4.0	51.7 ± 5.0	49.0 ± 4.3
4	56.3 ± 10.5	74.3 ± 15.8	36.6 ± 13.0	44.0 ± 7.9	46.5 ± 10.7	46.3 ± 9.9
5	71.0 ± 9.4	75.6 ± 8.4	75.9 ± 22.4	58.8 ± 8.5	58.3 ± 9.0	56.2 ± 7.5
6	71.0 ± 14.2	79.4 ± 9.7	N/A	54.2 ± 7.7	57.7 ± 11.3	54.0 ± 7.1
7	67.7 ± 11.0	75.4 ± 14.1	68.3 ± 19.5	57.1 ± 9.0	56.8 ± 10.1	56.2 ± 9.9
8	62.4 ± 10.6	73.5 ± 12.2	55.0 ± 17.1	48.0 ± 5.7	51.7 ± 9.4	49.2 ± 7.7
average	67.3	78.9	57.1	52.5	55.0	53.1

Table 2

Segment-based analysis for the proposed 3-parameter fit with 27 echoes. The results show that the range of variation for average T_2 values across the six mid-ventricular myocardial segments is 4.2 ms. The range of variation for the B/A parameter is 0.01. The value predicted for B/A by Equation [6] for the given sequence parameters is 0.13 (subj = subject, seg = segment).

	T_2 (ms)						B/A					
Subj\Seg	**1**	**2**	**3**	**4**	**5**	**6**	**1**	**2**	**3**	**4**	**5**	**6**
1	70	67	60	56	51	55	0.13	0.18	0.20	0.19	0.21	0.18
2	60	56	58	60	55	56	0.17	0.16	0.18	0.17	0.17	0.17
3	53	53	49	51	52	52	0.17	0.16	0.15	0.14	0.16	0.16
4	43	39	43	47	46	41	0.18	0.20	0.18	0.14	0.13	0.14
5	59	58	59	59	53	56	0.09	0.10	0.13	0.12	0.12	0.13
6	53	56	55	53	52	50	0.16	0.13	0.13	0.15	0.15	0.15
7	58	53	54	59	55	61	0.12	0.10	0.12	0.12	0.12	0.14
8	58	53	54	59	55	61	0.12	0.10	0.12	0.12	0.12	0.14
average	56.8 ± 7.6	54.3 ± 7.6	53.8 ± 5.6	55.5 ± 4.7	52.6 ± 3.2	54.2 ± 6.7	0.14 ± 0.03	0.14 ± 0.04	0.15 ± 0.03	0.14 ± 0.03	0.15 ± 0.03	0.15 ± 0.02